Journal of Physics D:
Applied Physics

PAPER • **OPEN ACCESS**

Secondary electron emission yield of Teflon®, Kapton®, RT/Duroid® and ferrite under induced surface charging states

To cite this article: L Esteve *et al* 2025 *J. Phys. D: Appl. Phys.* **58** 425304

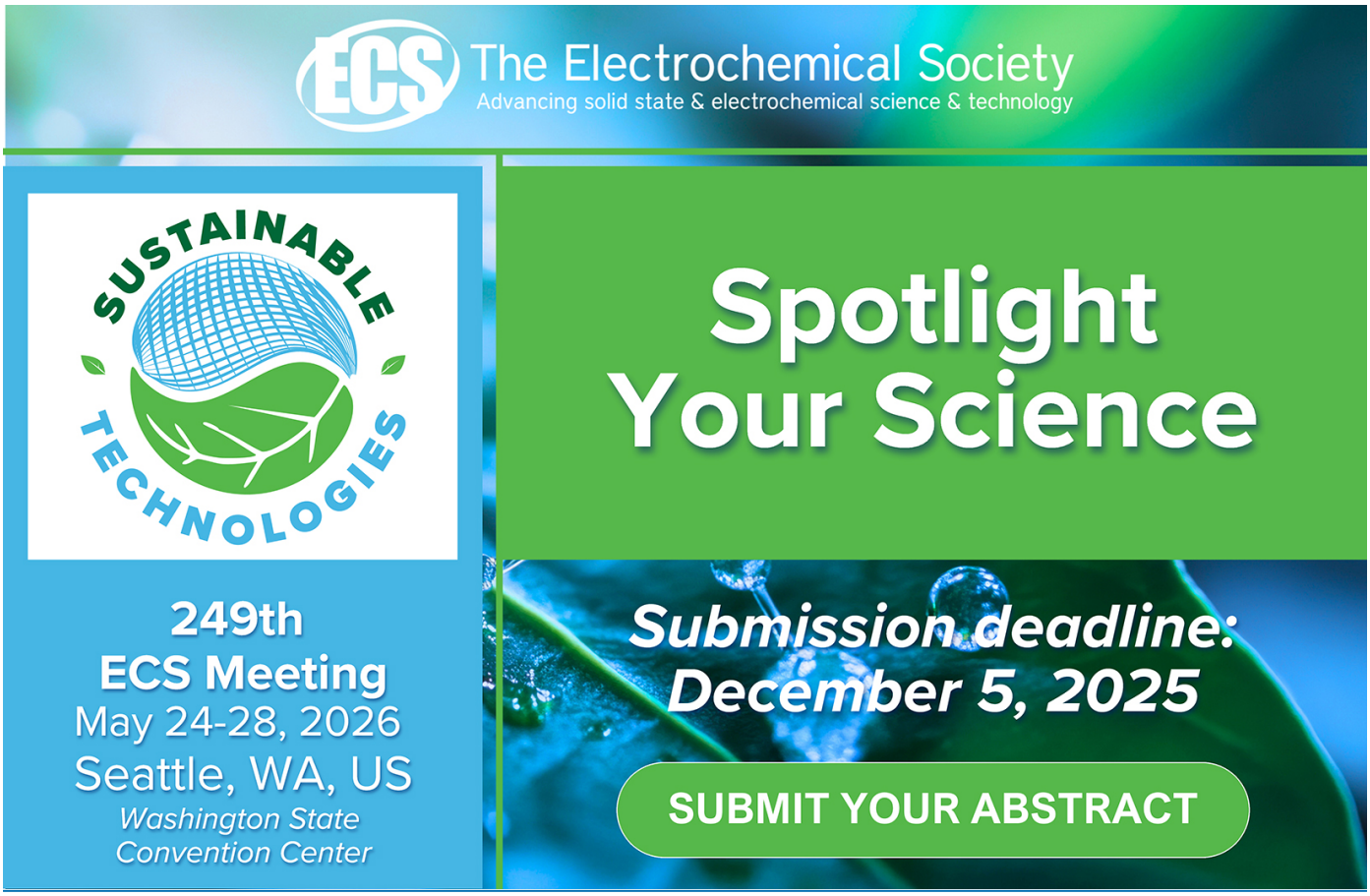

OPEN ACCESS
IOP Publishing
Journal of Physics D: Applied Physics
J. Phys. D: Appl. Phys. **58** (2025) 425304 (10pp)
https://doi.org/10.1088/1361-6463/ae0fa5

Secondary electron emission yield of Teflon®, Kapton®, RT/Duroid® and ferrite under induced surface charging states

L Esteve[1,2,*], R Mata[2,3], O Monerris[2], C Alcaide[1], C Miquel[4] and V E Boria[1,2]

[1] Institute of Telecommunications and Multimedia Applications (iTEAM), Escuela Técnica Superior de Ingeniería, Polytechnic University of Valencia, Camino de Vera s/n, 46022 Valencia, Spain
[2] ValSpace Consortium, Ciudad Politécnica de la Innovación, 8G Building, Access B, Floor B, Camino de Vera s/n, 46022 Valencia, Spain
[3] Material Science Institute (ICMUV). University of Valencia, C/Catedrático José Beltrán 2, 46980 Paterna, Valencia, Spain
[4] European Space Agency, ESTEC, Noordwijk, The Netherlands

E-mail: laura.esteve@val-space.com

Received 9 June 2025, revised 22 September 2025
Accepted for publication 6 October 2025
Published 17 October 2025

Abstract

Dielectric materials are increasingly common in modern satellite payloads due to their advantageous properties, such as the large mass and volume reduction can be achieved when they are used in radiofrequency (RF) equipment. However, the presence of dielectric materials in the output high-power section of RF payloads requires careful study of their influence on the multipactor performance, and therefore, their secondary electron emission yield (SEY). This characterization in dielectrics is nowadays a challenging and time-consuming practice relying on the electrical charge neutralization before each measurement. However, surface charging of dielectrics can be developed during the satellite operation and can significantly influence their SEY properties, thereby affecting the multipactor threshold. For the first time, this study succeeds in providing the experimental SEY curves of Teflon®, Kapton®, Rogers RT/Duroid®, and Ferrite under controlled and induced surface charging states. These materials were studied due to their common employment in satellite communication devices. Using an electron gun working in combination with a Kelvin probe system, it was possible to characterize the SEY characteristics of the materials after inducing different charge levels on their surface. From the results, it can be concluded that surface charging has a significant effect in lowering the SEY levels. Nevertheless, this effect could only be observed in materials with high electrical resistivity, since the surface charge rapidly dissipated in materials with lower electrical resistivity before the SEY measurement took place. Therefore, these findings provide valuable insights into the design and optimization of dielectric materials for space applications, giving an accurate overview of their SEY response under possible charging states in orbit.

* Author to whom any correspondence should be addressed.

Keywords: secondary electron emission yield, charging states, space materials, electrical resistivity, multipactor involving dielectrics

1. Introduction

In satellite communications, the payload equipment must comply with several requirements for space qualification, for instance, with radiofrequency (RF) power margins in microwave devices that are susceptible to multipactor discharge [1, 2]. This detrimental phenomenon occurs in vacuum conditions and depends on several parameters, such as the applied RF power level, the frequency of operation, the geometry of the device, or the materials involved in the design [3]. It begins when free, or primary electrons present inside the RF component are accelerated by the high-power electromagnetic fields and impact the component wall. Depending on their kinetic energy, they can be either backscattered or captured, transferring in this last case their energy to the electrons of the material, or secondaries, that can, in consequence, escape from the surface [4]. Once these secondary electrons reach the vacuum, they can be accelerated under certain conditions in the opposite direction, impacting again and releasing more electrons producing an avalanche effect, commonly known as multipactor discharge. This effect can trigger undesired responses, such as an increase in part of the RF signal level, an increase in the noise, or energy spreading in the harmonic frequencies. The consequences sometimes are dramatic, even causing damage to the RF payload or losing communication with the satellite. As supposed, multipactor discharge will strongly depend on the material involved in the telecommunication device.

In the last few years, the use of dielectric materials in satellite communications has become increasingly popular, since the size of passive microwave devices can be reduced by including them inside their structure [5]. However, the presence of dielectric materials in space hardware introduces additional effects and uncertainties compared with metallic materials, such as the accumulated and remaining charge on their surfaces [6]. It is well-documented that dielectric materials can get charged through mere friction with air [7], for instance, due to the air evacuation from inside the space components during the transition from atmospheric pressure to high vacuum during the satellite launch phase. Additionally, space weather or even the presence of the RF electromagnetic field, among other causes, can also charge the dielectric materials used in the satellite while it is in orbit. Consequently, dielectric components in orbiting RF devices can present an unknown surface charge level that might influence their secondary electron emission yield (SEY) properties, and therefore the multipactor breakdown power threshold [8]. Nevertheless, in the laboratory, the experimental SEY measurement in metals is relatively easy because the surface charge remains stable during the measurement, and the SEY measurement in dielectric materials is quite complicated and normally is referred to an electrical neutral state, which requires neutralization techniques at each step of the measurement process [9].

Under this problematic, since the SEY in dielectrics may induce positive or negative charge on their surface if the $\mathrm{SEY} > 1$ or $\mathrm{SEY} < 1$, respectively, causing, in consequence, a surface potential due to the accumulated static charge [10]. Recent studies have shown that as positive charge accumulates on the dielectric, the secondary electron yield profile decreases across the entire impact energy range [11, 12] due to the Coulomb attraction of the secondary electrons. Consequently, the SEY curve measured in the laboratory under neutral conditions may not reflect the real conditions of the dielectric in orbit, leading to an unreliable and non-realistic multipactor threshold estimation [13]. In this article, we present a study of the SEY properties for different dielectric materials under several well-controlled surface charging states, providing for the first time reliable experimental data to better model the multipactor behaviour in space components, thereby improving their design and reliability. In particular, the materials chosen for this investigation were PTFE (Teflon®) [14], Kapton® [15], RT/Duroid 5870® [16] (from now on, RT/Duroid®), and Ferrite [17]. These materials have been chosen mainly for their wide range of applications in the space industry. The most common use of Teflon® is for the insulation of wiring in aerospace, but it is also widely used in printed circuit boards and antennas [18, 19]. Teflon® has excellent dielectric properties, specifically low group velocity dispersion at microwave frequencies [20]. Another example of a substrate able to withstand space conditions is RT/Duroid®, which presents good behaviour up to Ka-band frequencies. Kapton® can be used for flexible printed circuits, as well as thermal blankets, among other spacecraft components [21]. Finally, ferrite materials consist of insulating magnetic oxides with moderate magnetization, high permeability, moderate to high permittivity, and low losses at microwave frequencies. Additionally, due to their intrinsic magnetism, these materials also provide non-reciprocal behaviour, which is essential in communications systems [17, 22]. Another relevant factor in selecting these materials is focused on their electrical resistivity, whose values are listed in table 1. This intrinsic property refers to their ability to resist the flow of electric current, narrowly related to the formation of remanent surface charging states. Thereby, in this investigation, materials with electrical resistivity from 10^4 to $10^{16}\ \Omega \cdot \mathrm{m}$ have been considered. The dielectric permittivity of each material is also indicated in the same table and will be used in the following sections.

Although dielectric materials can get charged positively or negatively, as has been mentioned above, this work is only focused on inducing positive surface charging states and their effects on the SEY curve, due to their direct influence on the multipactor breakdown prediction. These positive charging

Table 1. Electrical resistivity and relative dielectric permittivity of Teflon®, Kapton®, Rogers RT/Duroid 5870® and Ferrite.

Material	Resistivity, $\rho(\Omega \cdot \mathrm{m})$	Relative dielectric permittivity, ε_r
Teflon®	$>10^{16}$ [14]	2.1 [14]
Kapton®	10^{14} [15]	3.4 [15]
RT/Duroid®	10^{11} [16]	2.3 [16]
Ferrite	10^{4} [22]	15.1 [17]

states are generated when SEY > 1, when the multipactor discharge is more likely to be initiated.

2. Experimental setup and procedures

The SEY coefficient is the ratio between the number of secondary electrons emitted from the surface of a given material and the number of incident primary electrons over this surface at a given energy and angle in field-free conditions. In this work, the incident angle has been constrained to normal incidence, and the experiments were performed at room temperature (22 °C). The total SEY curve is expressed as a function of the kinetic energy of the primary electrons and the main parameters that characterize the SEY curve are: the maximum SEY value, σ_m; its corresponding energy, E_m; and the first and second cross-over energies, E_I and E_{II}, corresponding to SEY $= 1$. Representative SEY curves can be seen with their corresponding parameters in [4].

The European ESA/VSC High Power Space Materials Laboratory [23], and its SEY facility used for the experiment, is placed inside a 10.000 class (ISO 7) clean room. The nominal temperature and humidity of the clean room during the experiment were 22 °C ± 1 °C and 50% ± 10%, respectively. The facility features an ultra-high vacuum chamber with a pumping system that can reach pressure levels in the range of 10^{-8} mbar. Before conducting the measurements, a Platinum sample was used to validate the operational performance of the SEY facility and demonstrate its nominal operation and reproducibility. Several measurement techniques can be used to experimentally measure these SEY curves, depending on the nature and electrical resistivity of the material under test [24, 25]. However, due to the dielectric nature of the materials under study in this article, the SEY measurements have been conducted following the capacitive method, pulsing a primary electron gun, Kimball Physics model ELG-2/EGPS-1022, as described in [8]. This electron gun can generate electron radiation with kinetic energies from 0 to 2000 eV, with an accurate intensity between 1 nA and 30 μA. However, our SEY curves are restricted to energies between 0 and 600 eV. Accordingly, very small electron doses ($<10^7$ electrons) are sent to the material samples under study to reduce charging effects during SEY measurements. Then, the SEY coefficient is calculated using the following formula:

$$\mathrm{SEY} = \frac{Q_\sigma}{Q_p} = 1 - \frac{Q_s}{Q_p} \tag{1}$$

where Q_p represents the total primary charge obtained by time-integrating the incident pulse current using a Faraday cup biased at +56 V, Q_s is the image charge obtained by time-integrating the current through the holder at the rear side of the sample, and Q_σ is the charge produced by the secondary electrons. Since the primary charge equals the sum of Q_σ and Q_s, the equation can be reformulated as shown in the second equality of equation (1), containing easily measurable terms.

In parallel, a Kelvin Probe system (KP Technology UHV Kelvin Probe Series 10) equipped with a circular probe of 20 mm diameter, to ensure that the whole radiated area is detected, is also configured to work in vacuum conditions simultaneously with the e-gun, with the aim of characterizing the induced surface charging states. In this sense, the electron gun parameters remain constant to ensure the reproducibility of the electron beam spot and the reproducibility of the induced surface charging state in the whole range of primary electron energy. This equipment provides the induced voltage that the accumulated charge produces, and the accumulated charge at the sample surface was calculated by using the following formula [26]:

$$Q_c = C\Delta V \tag{2}$$

where $\Delta V = V_f - V_i$ is the potential difference induced by the primary electron pulse before (i) and after (f) primary electron radiation, and C is the capacitance of the sample that can be experimentally calculated. The facility also includes a deuterium ultra-violet (UV) lamp (HAMAMATSU L15094), which provides photons with wavelengths from 115 to 400 nm. This is used to electrically neutralize the surface charge of the sample under analysis.

The general procedure to induce the surface charging states and measure the SEY curves starts by introducing the material sample into the vacuum chamber at 10^{-8} mbar, while it is contacted to a metal holder. Firstly, it is electrically neutralized by means of UV radiation for 2 min while it is grounded. Secondly, KP measurements were conducted to confirm the sample's neutral electrical status. If the measurements showed a remnant charge, the irradiation process was repeated. In the next step, a determined charging state was induced on the sample surface by sending a pulse of primary electrons with an energy of 300 eV, around the maximum SEY coefficient, to the sample while it was biased at −28 V. Then, the voltage generated by the charging state was measured using the KP system to obtain the corresponding charge using equation (2). Finally, the SEY properties are measured, and the sample is again electrically neutralized, the primary electron is changed, and the procedure is again repeated for all the primary energy range considered during the experiment.

Figure 1 depicts a schematic representation of the setup used for this work. Path (a) was configured to induce the charging states and measure the SEY properties, while path (b) was used to evaluate the system's capacitance as explained in [8]. Path (c) is used to measure the primary charge, Q_p, placing the Faraday cup in front of the electron gun biased at +57 V.

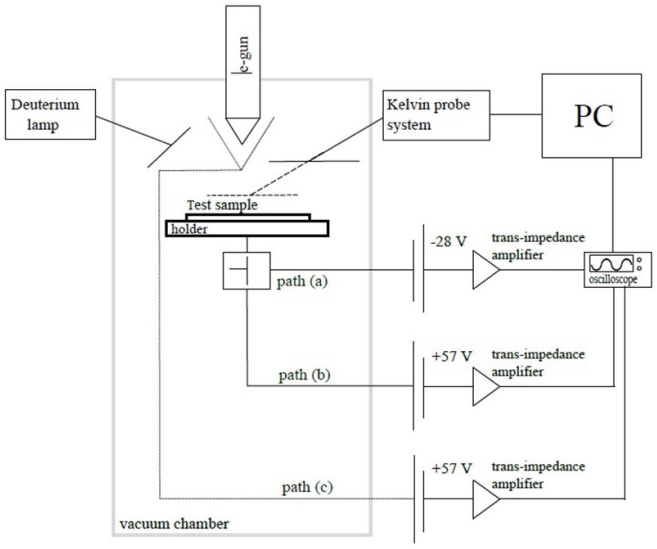

Figure 1. Schematic representation of the setup used for inducing charging states and measuring the SEY properties on the materials under study.

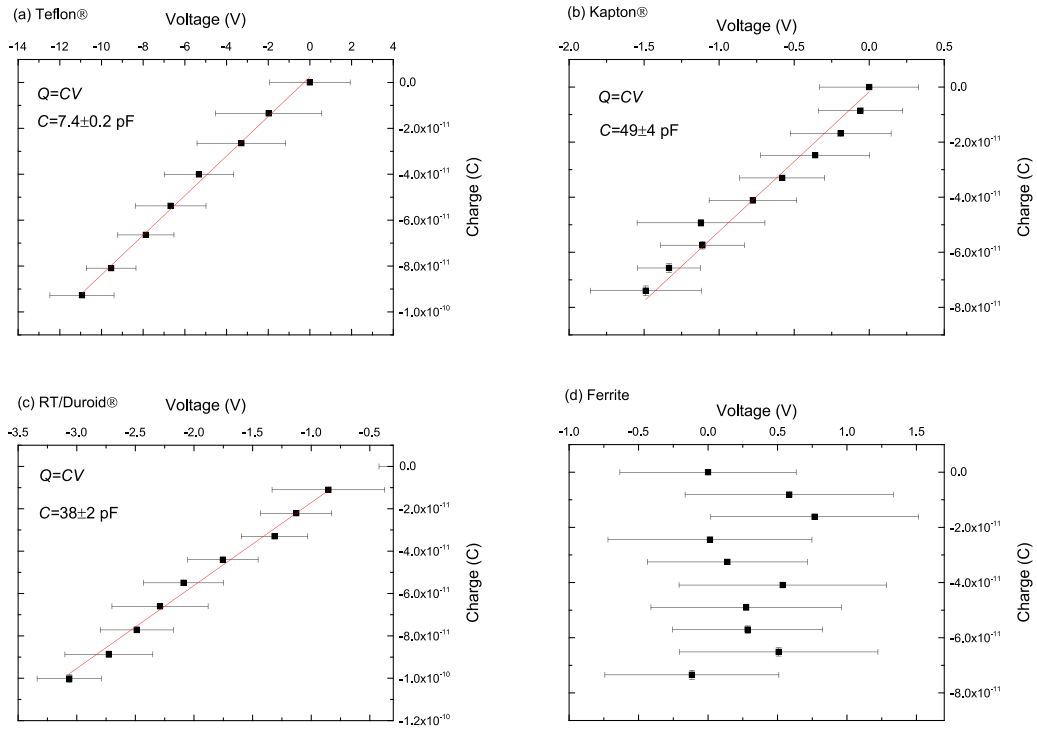

Figure 2. Induced charge versus the measured voltage at the sample surface for Teflon® (a), Kapton® (b), RT/Duroid® (c) and Ferrite (d). The obtained capacitance is shown inside each graph.

3. Samples characterization

In order to experimentally measure the capacitance of each sample under study, we applied the following procedure explained in detail elsewhere [27]: first, a primary electron charge is measured using the electron gun faraday cup while it is biased at +57 V; second, the same charge pulse with an energy below the first cross over is sent to the sample surface biased at +57 V to ensure that all the primary electron are absorbed by the material; and finally, the surface potential is measured by means of the KP system. These steps are repeated by varying the primary electron dose. Figure 2 shows the induced charge versus the corresponding measured voltage for Teflon® (a), Kapton® (b), RT/Duroid® (c) and Ferrite (d), respectively. The capacitance of each sample was extracted from the slope of the linear fitting. Furthermore, considering previous analysis of this facility [8], an amount of $C_0 = (1.20 \pm 0.07)\ 10^{-12}$ F corresponding to the facility parallel capacitor contribution, was subtracted from the measured capacitance to obtain the material sample capacitance only.

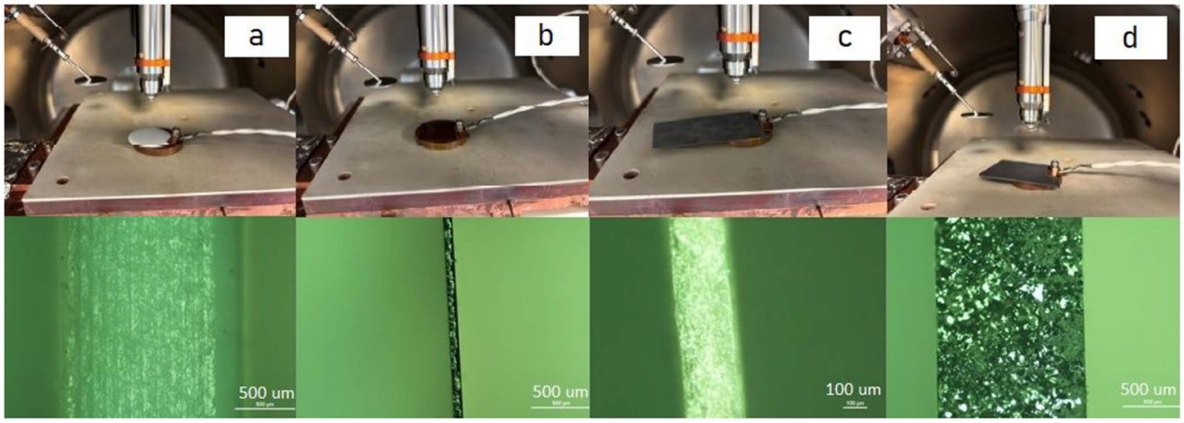

Figure 3. In rows, pictures of Teflon®(a), Kapton®(b), RT/Duroid®(c) and Ferrite (d) inside the vacuum chamber (top) and sample thickness measurements in the microscope (bottom).

Table 2. Calculated capacitance, thicknesses and estimated radius of the radiated area for the materials used in this work.

Material	Capacitance, C (pF)	Sample Thickness, d (m)	Radius, r (m)
Teflon®	7.4 ± 0.2	$(1.50 \pm 0.15)\cdot 10^{-3}$	0.013 ± 0.002
Kapton®	49 ± 4	$(7.5 \pm 0.8)\cdot 10^{-5}$	0.006 ± 0.001
RT/Duroid®	38 ± 2	$(2.6 \pm 0.3)\cdot 10^{-4}$	0.012 ± 0.002
Ferrite	NA[a]	$(1.26 \pm 0.13)\cdot 10^{-3}$	NA[a]

[a] This radius could not be calculated because no relation between Q and V was found for this material, see figure 4(d).

Therefore, only the sample capacitance is shown in table 2 and in the inset of the graphs. On the other hand, the thickness of the samples was measured prior to the experiment using a calibrated optical microscope and is also listed in table 2. Figure 3 shows, in the upper row, the samples inside the vacuum chamber ready to be measured, and in the bottom row, their microscope pictures with the corresponding scale bars.

With the aim of verifying the reliability of the experiment, i.e. the radiated area with primary electrons is completely covered by the KP tip area, the experimental capacitance is used to calculate the electron gun radiated area on the sample surface, considering it as a simple parallel plate capacitor modelled with the formula:

$$C - C_0 = \varepsilon \frac{A}{d} \tag{3}$$

where d is the sample thickness, A is the radiated area by the electron gun beam, and $= \varepsilon_0 \varepsilon_r$ refers to the dielectric permittivity of the material. The calculated radius of the radiated area is listed in the last column of table 2 for each material. These values are intermediate between the KP tip diameter (20 mm) and the sample dimensions (more than 30 mm). Although they should be smaller than the KP tip size, the discrepancies might be attributed to edge effects that are not included in this simple theoretical model. In addition, it must be considered the Gaussian shape of the electron gun beam, wherein the major percentage of the electrons are concentrated in the spot centre, and a very small percentage of them would impact near the border of the radiated area. Therefore, based on this argument, in the measured area by the KP tip, the induced charge can be considered constant.

4. Experimental results and discussion

Following the procedure explained in the previous sections, the SEY properties under different induced charging states were investigated. For that purpose, several charging states were induced by sending different primary electron doses to the samples. Figure 4 shows representative pulses of the intensity detected in the rear sample side through the metallic holder, in red, green, blue, and light blue of the induced charging states on the Teflon® (a), Kapton® (b), RT/Duroid® (c), and Ferrite (d) samples. The graphs represent the current intensity as a function of time, where the pulses have been shifted to improve the clarity of the plots. To generate this induced charge, primary pulses were sent with an energy of 300 eV to take advantage of the SEY properties greater than 1: for the materials used in this work, the SEY > 2 for this primary energy in neutral state conditions. The integrated charge from each pulse is shown in the legend, where: Q_p corresponds to the primary charge measured with the Faraday cup bias at $+57$ V used to induce the charging states, only shown for the highest one (in grey); and Q_c is the induced charge corresponding to the charging state measured by the capacitive method while the sample was bias at -28 V. The primary charge dose was adjusted by varying the

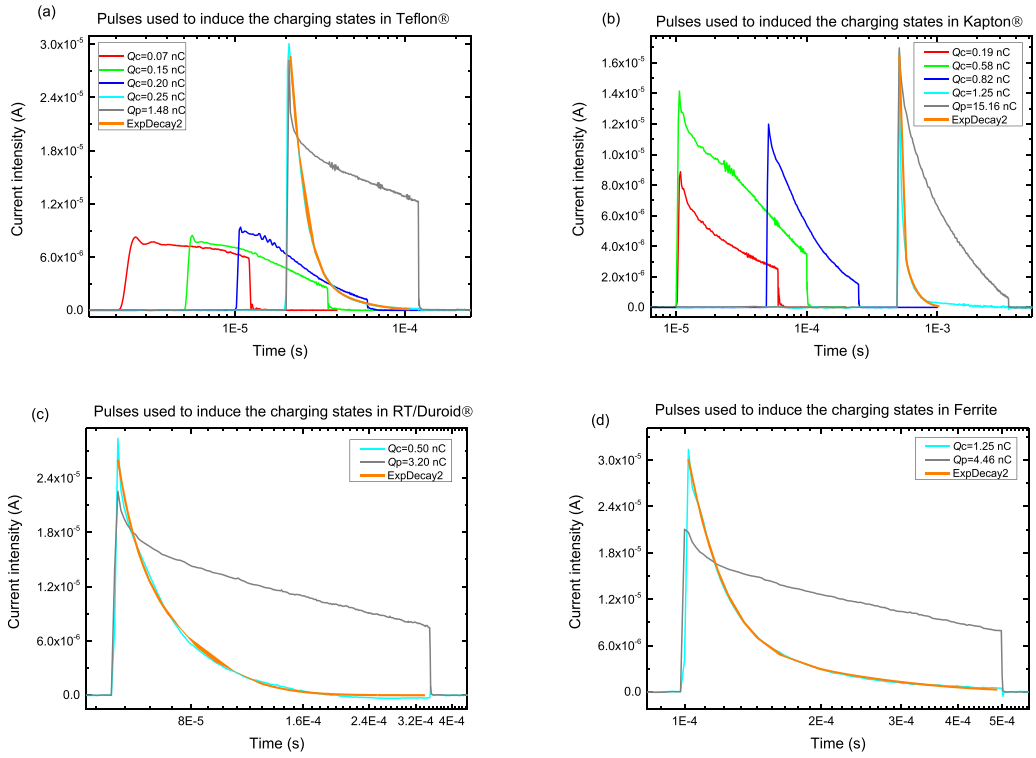

Figure 4. Primary pulses (Q_p) for the highest charging state in grey, and representative pulses of each induced charge state (Q_c) for Teflon® (a), Kapton® (b), RT/Duroid® (c) and Ferrite (d).

pulse width and the electron gun cathode emission electron intensity.

Comparing the representative primary pulse (in grey) used to induce the highest charging state (light blue pulse), it can be observed how the generated current for the light blue pulse and the grey pulse differs dramatically: when the light blue current tends to zero throughout the grey pulse duration, there are still arriving primary electrons to the sample surface. Therefore, during this primary pulse width (grey pulse) the sample material is electrically saturated [28]. In consequence, lower doses were sent to induce other measurable charging states. Note that for RT/Duroid® and Ferrite, only the saturated charging state was possible to be induced because their lower electrical resistivities do not retain the charges at the sample's surface due to fast recombination processes.

Since the materials present a behaviour like a capacitor during a transitory phase while they are charging, the intensity as a function of time for the higher charging state (light blue pulse) was fitted using a capacitor model. The fittings are shown in the same graphs of figure 4 with an orange line. However, a double exponential decay was needed to fit the experimental data. Therefore, for all the materials, two decay times ($\tau = RC$) were found: one short, τ_1, which can be attributed to faster recombination of charges; and the other, τ_2, to recombination of charges that need longer times. Both decay times were transformed into their corresponding resistance through the capacitance of each material and represented as a function of their resistivity in figure 5 with black squares and red dots, respectively. No data could be obtained for the Ferrite due to its non-capacitive behaviour. Note that both axes of the plot

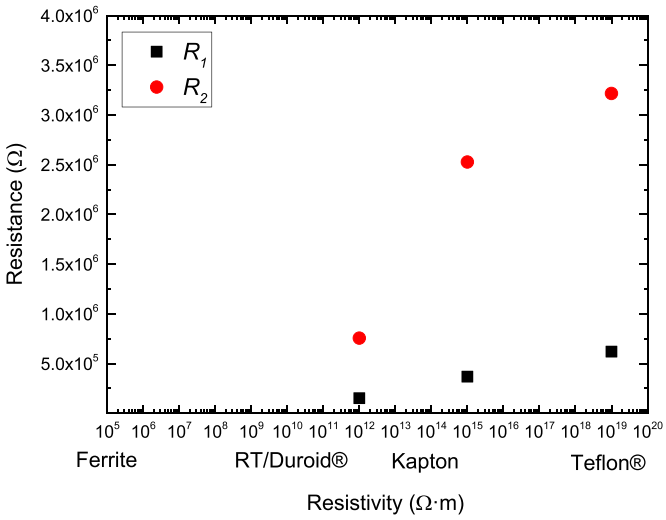

Figure 5. Calculated sample resistance using the decay times and their corresponding capacitance as a function of their resistivity.

are represented on a logarithmic scale. As expected, both resistances decrease as the resistivity decreases. Regarding R_1, corresponding to τ_1, it remains in the range of 10^5 Ω, and its variation with the resistivity might be related to the depth from the surface where an internal charge layer is formed, being located deeper for thicker samples according to recent theoretical studies [29]. This layer is expected to be located close to the metallic sample holder, and therefore, shorter times are needed for the charges to be recombined. From τ_2, higher values of R_2

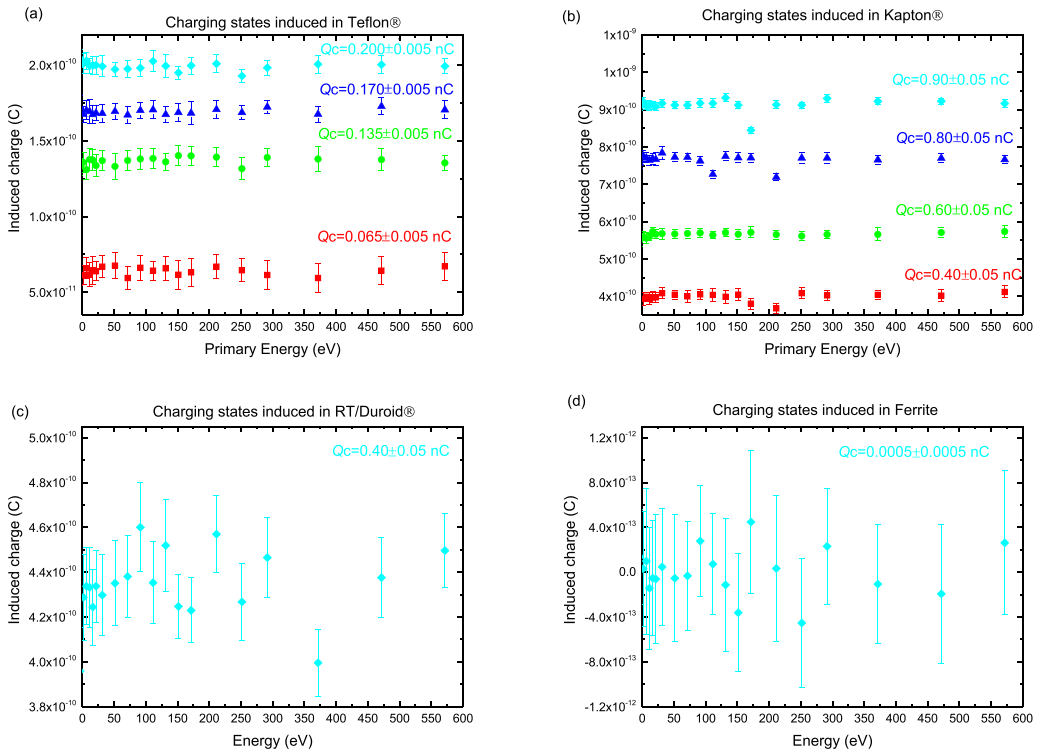

Figure 6. Charge states Q_c measured with the KP technique at the sample surface for Teflon® (a), Kapton® (b), RT/Duroid® (c) and Ferrite (d).

were obtained, which are attributed to the recombination of charges generated at the sample surface by the induced charging states close to the sample surface. Then, τ_2 will depend on the depth of this layer of charge and the electrical conductivity of the material. To understand the behaviour of the calculated resistances, it must be considered that the induced charging state at the sample surface not only depends on the impinging primary charge intensity but also on the type of material, as demonstrated in [30]. These considerations, in addition to the complexity of accurately knowing the radiated area A, explain the non-linear dependence between resistance and resistivity ($R = \frac{d}{A}$). However, these data support the impossibility of inducing a remaining surface charging state in materials with lower resistivities than $10^{11}\ \Omega \cdot \mathrm{m}$.

Considering that the sample materials behave as a capacitor, Q_c measured with pulses like the representative ones of figure 4 should be equal to the induced charge at the radiated sample surface. However, due to recombination processes according to the material electrical resistivity, the induced charging states were characterized by measuring Q_c at the sample surface using the KP tip, which is shown in graphs of figure 6 for the whole primary energy range using the same colour than the corresponding and representative pulses of figure 4. Hence, it can be observed that Q_c obtained with the KP for the same charging states are slightly lower than the corresponding values obtained by integrating the pulses obtained at the rear side of the sample surface. This trend is explained by the activation of charge recombination processes according to the electrical conductivity of each material, because these measurements with the KP tip were carried out after sending the primary electron dose. The graph includes the corresponding average of the induced surface charging state, Q_c, for the whole primary energy range under study. These values were calculated using the measured surface potential with the KP system and the corresponding capacitance of table 2. As can be noticed in figure 6, for materials with high resistivity: Teflon® (a) and Kapton® (b), it was possible to induce reproducible several charging states between the neutral state and the saturated charging state (light blue). However, as electrical resistivity decreases, the capability of the material to keep the induced charge on the material surface drastically decreases. Actually, it was impossible to maintain a constant accumulated charge at the sample surface during the SEY measurement, increasing its dispersion for the whole primary energy range, as can be observed in figures 6(c) and (d).

Figure 7 shows the SEY curves obtained under their corresponding induced charging states for all the materials under study. The SEY curve obtained under neutral states, which are indicated with black spheres, agrees well with values in the literature [31, 32].

For Teflon® and Kapton®, with the highest electrical resistivities, the SEY curves show a clear trend as the charging state increases: σ_m and E_m decrease, while E_I increases. This behaviour can be understood using an electron-hole model, where part of the secondary electrons are attracted by the positive potential generated at the sample surface and return to the material surface [33], and in consequence, the SEY is modified. On the one hand, the number of secondaries is reduced, decreasing σ_m and increasing E_I. Some of the primary electrons may penetrate below this positive surface potential layer

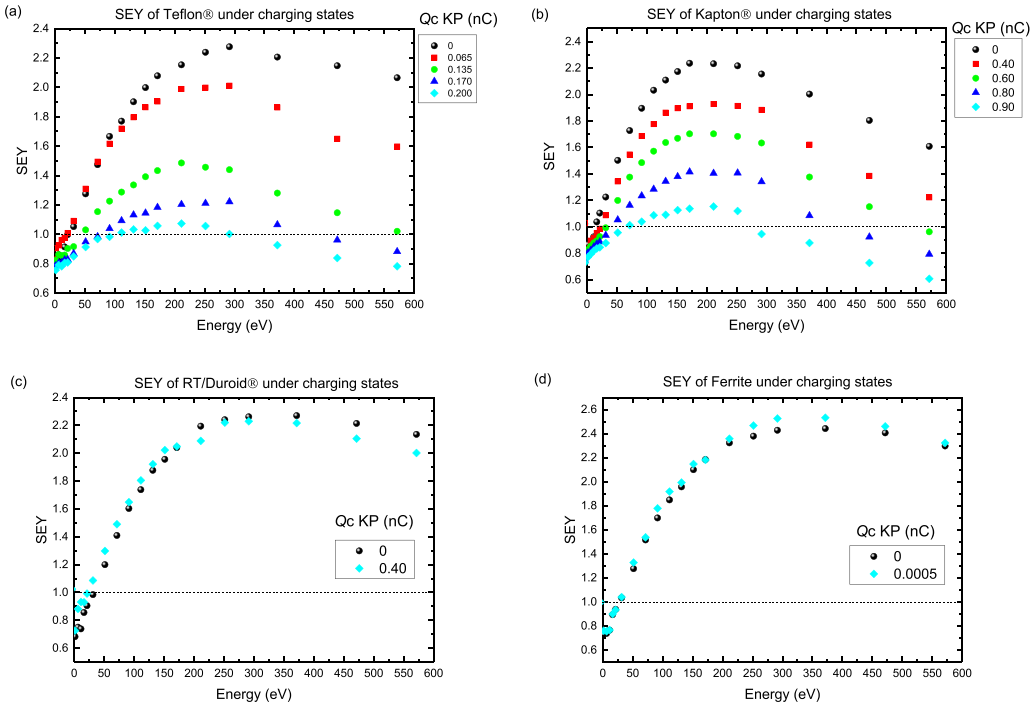

Figure 7. SEY curves under induced charge stated Q_c for Teflon®(a), Kapton®(b), RT/Duroid®(c), and Ferrite(d).

[10, 34], creating a negative charge distribution beneath the positive potential, and therefore producing a dipolar-like configuration. This negative layer produces a new electron charge balance with the positive charging state that might shift the E_m parameter accordingly. The depth of this negative charge layer will mainly depend on the primary electron energy, which has been maintained constant at 300 eV in this work, and the material properties.

On the contrary, RT/Duroid® and Ferrite samples present a completely different behaviour. The SEY curves obtained for these materials, whose electrical resistivities are lower than 10^{11} Ω m, were equivalent for both the neutral state and the state induced for charging saturation (light blue). These results show that the induced positive charge generated at the sample surface vanished before the SEY measurement took place due to rapid charge recombination processes.

Finally, it is worth highlighting that these results contribute to the multipactor threshold prediction in the presence of dielectric materials. In orbit, the primary electrons inside the RF equipment impact on the walls (metal and dielectrics) with a huge range of energy. This work focuses on inducing charging states for only one primary energy, but the trend of the SEY curve when the charging state becomes positive can be extrapolated to the energies where SEY > 1. However, the dielectric materials present inside the RF chain may be charged positively or negatively, depending on the SEY parameter of the curve at the corresponding primary energy. Although this scenario is complex to model, the positive charging states are the most probable when a multipactor discharge triggers. During the discharge, the electron population grows dramatically, feeding the positive voltage on the surface, and thus reducing the SEY curve depending on the charging state reached. Additionally, from the multipactor point of view, a second effect arises when a dielectric gets charged: the potential generated in the material surface creates an electrostatic field. The presence of this direct current (DC) field could deviate the electron trajectories and therefore impact the multipactor threshold. This fact, together with the SEY curve reduction, highlights the importance of this work in the field of multipactor discharge prediction.

5. Conclusions

Different positive surface charging states in Teflon®, Kapton®. For the RT/Duroid® and Ferrite were induced. Additionally, SEY properties were obtained under these surface charging states. For the measurements, a KP system was installed in a vacuum chamber to work in combination with an electron gun. The KP was used to evaluate the induced surface potential, and the SEY curves were obtained using the well-known capacitive method. We were able to induce different charging states in Teflon® and Kapton® due to their high electrical resistivities. However, in RT/Duroid® and Ferrite, with electrical resistivities lower than 10^{11} Ω m, it was found that the charge could not be retained on the material surface, obtaining SEY curves equivalent to the neutral state.

Considering that the sample materials under electron radiation behave as a capacitor, it was found a double transitory decay: one attributed to the migration of charges from the internal charge layer close to the metallic holder in the rear side of the sample; and the other, to charge recombination between a negative charge layer created by primary electrons close to the radiated sample surface and the positive charging sate at

the sample surface. Both decay times strongly depend on the electrical resistivity of the material.

From the SEY curves obtained under induced positive charging states in materials with higher electrical resistivity, a clear trend in the main SEY parameters was found: σ_m and E_m decrease, while E_I increases. This trend is attributed to the coulombian attraction by the positive surface potential generated at the sample surface in combination with the dipolar-like behaviour of the formed negative charge close to the sample surface.

This work provides experimental results that contribute to a better understanding of the multipactor threshold in space components involving dielectrics. On the one hand, the SEY curves of several space materials are analysed under induced and controlled charging states. On the other hand, the DC field generated on the material surface can be accurately measured. Considering both parameters, a dramatic impact on the multipactor threshold prediction may occur, leading to erratic results if they are not considered in prediction models.

Data availability statement

The data cannot be made publicly available upon publication because they are owned by a third party and the terms of use prevent public distribution. The data that support the findings of this study are available upon reasonable request from the authors.

Acknowledgments

The authors would like to thank the European ESA/VSC High Power Space Materials Laboratory for its contribution—a laboratory funded by the European Regional Development Fund—a way of making Europe. And, to the European Space Agency for the given support and funding through the research activity VSC/TEC/O/24/57/TASCHARG.

Author contributions

L Esteve 0009-0005-7636-9570
Conceptualization (supporting), Formal analysis (equal), Investigation (equal), Methodology (equal), Writing – original draft (lead), Writing – review & editing (equal)

R Mata 0000-0001-7087-3796
Conceptualization (lead), Formal analysis (equal), Investigation (equal), Methodology (equal), Supervision (lead), Writing – original draft (equal), Writing – review & editing (equal)

O Monerris 0000-0002-2247-5192
Writing – review & editing (supporting)

C Alcaide 0000-0001-5772-9204
Writing – review & editing (supporting)

C Miquel 0009-0007-6460-2966
Funding acquisition (lead), Writing – review & editing (supporting)

V E Boria 0000-0001-7150-9785
Funding acquisition (supporting), Supervision (lead), Validation (lead), Visualization (lead), Writing – review & editing (lead)

References

[1] European Cooperation for Space Standarization (ECSS) 2020 Multipactor design and test (ECSS-E-ST-20-01C) ESA-ESTEC requirements & standards division noordwijk
[2] Vaughan J R M 1988 Multipactor *IEEE Trans. Electron Devices* **35** 1172–80
[3] de Lara J, Perez F, Alfonseca M, Galan L, Montero I, Roman E and Garcia-Baquero D R 2006 Multipactor prediction for on-board spacecraft RF equipment with the MEST software tool *IEEE Trans. Plasma Sci.* **34** 476–84
[4] Scholtz J J, Dijkkamp D and Schmitz R W A 1996 Secondary electron emission properties *Philips J. Res.* **50** 375–89
[5] Sebastian M T, Silva M A S and Sombra A S B 2017 *Microwave Materials and Applications 2V Set* (Wiley) pp 1–51
[6] Kishek R A, Lau Y Y, Ang L K, Valfells A and Gilgenbach R M 1998 Multipactor discharge on metals and dielectrics: historical review and recent theories *Phys. Plasmas* **5** 2120–6
[7] Burgo T, Silva C, Balestrin L and Galembeck F 2013 Friction coefficient dependence on electrostatic tribocharging *Sci. Rep.* **3** 2384
[8] Belhaj M, Dadouch S, Duran-Venegas J A, Sinigaglia J and Mader P 2022 Charging effect, aging and storage conditions impact on SEY of dielectric materials for flight hardware MULCOPIM hal-03931072
[9] Mata R, Cros A, Gimeno B and Raboso D 2024 Secondary electron emission yield in thick dielectric materials: a comparison between Kelvin probe and capacitive methods *J. Appl. Phys.* **57** 405302
[10] Olano L and Montero I 2020 Energy spectra of secondary electrons in dielectric materials by charging analysis *Results Phys.* **19** 103456
[11] Belhaj M, Tondu T and Inguimbert V 2009 Experimental investigation of the effect of the internal space charge accumulation on the electron emission yield of insulators submitted to e-irradiation: application to polycrystalline MgO *J. Phys. D: Appl. Phys.* **42** 145306
[12] Belhaj M, Paulmier T, Hanna R, Arnaout M, Balcon N, Payan D and Puech J 2014 Charging behavior of Al_2O_3 and AlN under positive and negative charge injection using a kV electron beam *Nucl. Instrum. Methods Phys. Res. B* **320** 46–50
[13] Sorolla E, Belhaj M, Sobrim J and Puech J 2017 New multipactor dynamics in presence of dielectrics *Phys. Plasmas* **24** 103508
[14] Teflon® PTFE Dupont®, properties handbook (available at: www.rjchase.com/ptfe_handbook.pdf) (Accessed 09 January 2025)
[15] KAPTON® Corona resistant; ELECTRICAL, CR Takes. Kapton® *Stress* vol 10p 2
[16] Rogers Corporation RT/duroid® 5870/5880 Data sheet (available at: https://rogerscorp.com/advanced-electronics-solutions/rt-duroid-laminates/rt-duroid-5880-laminates) (Accessed 09 January 2025)
[17] Cardona J J V, Melgarejo-Lermas J C, Esbert V E B, Guglielmi M, Cambroreno M D R M, Mangada M S R and Mata-Sanz R 2019 Experimental validation of multipactor effect for ferrite materials used in L- and S-band nonreciprocal microwave components *IEEE Trans. Microw. Theory Tech.* **67** 2151–61

[18] Paillard M, Bodereau F, Drevon C and Guyon P 2005 Multilayer RF PCB for space applications: technological and interconnections trade-off *European Gallium Arsenide and Other Semiconductor Application Symp.* (https://doi.org/10.1109/EUMC.2005.1610270)
[19] Islam M T, Cho M, Samsuzzaman M and Kibria S 2015 Compact antenna for small satellite applications *IEEE Antennas Propag. Mag.* **57** 30–36
[20] Abdel-Wahab W M, Busuioc D and Safavi-Naeini S 2010 Low cost planar waveguide technology-based dielectric resonator antenna (DRA) for millimeter-wave applications: analysis, design, and fabrication *IEEE Trans. Antennas Propag.* **58** 2499–507
[21] Dahalan A H, Aziz M Z A A, Othman M A, Nornikman H and Ibrahim S 2019 Kapton® based antenna simulation analysis for smart system *Int. J. Integr. Eng.* **11** 286–91
[22] Harris V 2012 Modern microwave ferrites *IEEE Trans. Magn.* **48** 1075–104
[23] European ESA-VSC High Power Space Materials Laboratory ValSpace Consortium (available at: www.val-space.com/en/esa-vsc-european-high-power-space-materials-laboratory/)
[24] Balcon N, Payan D, Belhaj M, Tondu T and Inguimbert V 2012 Secondary electron emission on space materials: evaluation of the total secondary electron yield from surface potential measurements *IEEE Trans. Plasma Sci.* **40** 282–90
[25] Hessel R and Gross B 1992 Escape depth of secondary electrons from electron-irradiated polymers *IEEE Trans. Dielectr. Electr.* **27** 831–4
[26] Tondu T, Belhaj M and Inguinbert V 2011 Electron-emission yield under electron impact of ceramics used as channel materials in Hall-effect thrusters *J. Appl. Phys.* **110** 093301
[27] Fitting H-J and Touzin M 2010 Time-dependent start-up and decay of secondary electron emission in dielectrics *J. Appl. Phys.* **108** 033711
[28] Gross B and Hessel R 1991 Electron emission from electron-irradiated dielectrics *IEEE Trans. Dielectr. Electr.* **26** 18–25
[29] Feng G, Liu L, Cui W, Wang R and Hu T 2019 Transient characteristics of charging effects due to e-beam irradiation: a method of SEY-based charging balance mode *IEEE Trans. Plasma Sci.* **47** 3783–9
[30] Sun G-Y *et al* 2024 Investigation of the dynamic charge transport behaviors under electron beam irradiation of advanced insulation materials for aerospace applications *TechRxiv* (https://doi.org/10.36227/techrxiv.171778800.00606156/v1)
[31] Yang J, Cui W, Li Y, Miao G and Wang Q 2019 Study on secondary electron emission of high power microwave ferrite materials *2019 Joint Int. Symp. on Electromagnetic Compatibility, Sapporo and Asia-Pacific Int. Symp. on Electromagnetic Compatibility (EMC Sapporo/APEMC)* pp 218–21
[32] Burke E A 1980 Secondary emission from polymers *IEEE Trans. Nucl. Sci.* **27** 1759–64
[33] Hoffmann R, Dennison J R, Thomson C D and Albretse J 2008 Low-fluence electron yields of highly insulating materials *IEEE Trans. Plasma Sci.* **36** 2238–45
[34] Cazaux J 2006 e-Induced secondary electron emission yield of insulators and charging effects *Nucl. Instrum. Methods Phys. Res. A* **244** 307–22